

# Large earthquakes follow highly unequal ones

Sudip Sarkar<sup>1,\*</sup> and Soumyajyoti Biswas<sup>1,†</sup>

<sup>1</sup>*Department of Physics, SRM University - AP, Amaravati, Andhra Pradesh - 522240, India*

It was conjectured for a long time that the tectonic plates are in a self-organized state of criticality and that the Gutenberg-Richter law is a manifestation of that. It was recently shown that for a system near criticality, the inequality of their responses due to external driving would sharply rise and show universal behavior that could indicate proximity of the system to a critical point. As a result, measures such as the Gini and Kolkata indices that quantify inequality, can also serve as indicators of imminent criticality and that of diverging (system spanning) responses. In the context of earthquakes, such a large response would correspond to events of high magnitudes. In this work, we show with numerical simulations and seismic data analysis that large earthquake events have a tendency to follow events that are highly unequal, similar to the case of a system near a critical point. Therefore, a continuous monitoring of the inequality indices of the earthquake time series could be useful for hazard estimates. We have applied this framework to models of earthquakes as well as to the earthquake time series from various tectonically active regions, such as North America, Southern Japan, parts of South-East Asia and Indonesia. The findings also indicate a quantitative estimate of the distance from criticality, when the tectonic plates are viewed as a self-organized critical system.

## I. INTRODUCTION

When tectonic plates move (at a very slow rate), they undergo a stick-slip motion that causes earthquakes when the stored potential energy is released due to a sudden slip event. While much is known through more than a century of studies related to the motions and the subsequent energy released in tectonic plates, its understanding still faces severe difficulties, particularly due to the inaccessibility of the regions of origin (often tens to hundreds of kilometers underground) [1]. However, the phenomenon of earthquake has fascinated researchers from various disciplines alike not only due to their devastating consequences, but also due to their remarkable regularities in the statistical sense [2].

Particularly, it is known that the earthquake magnitudes follow the Gutenberg-Richter law [3],  $\log_{10} N = a - bM$ , stating that the number of earthquakes ( $N$ ) of magnitude  $M$  is related to  $M$  exponentially ( $a$  and  $b$  are constants). It is also observed that the rate of aftershocks decays with time in a power-law  $n(t) = K/(t+c)^p$ , known as the Omori-Utsu law [4, 5]. There are other empirical laws about earthquake dynamics as well, which are verified using data analysis across various regions in the world. While a complete understanding of the mechanism behind the earthquake phenomenon is still lacking, the empirical observations have been useful in gaining insights into the earthquake dynamics, improving the prospective to model the phenomenon and to also aim for a forecasting possibility, which has so far largely evaded complete understanding.

There have been some efforts in searching for regularities in earthquake statistics that could potentially lead to hazard analysis. One such observation is the change in the exponent value ( $b$ ) prior to a large earthquake event [6–9]. This method follows from the stress dependence of avalanche size exponent in sheared rocks, and also in fracture. In such cases, the avalanche size exponent value decreases prior to a large event. In earthquake also, when expressed in terms of energy, the size distributions follow a power law. The values of the power law exponent (linearly related to the above mentioned  $b$ -value of GR law) decreases, if the events are sampled prior to a large event (see e.g., [8]). Also, other complexity measures prior to large earthquakes have been studied in recent years with the aim of possible forecasting (see e.g., [10–12]).

In this work, we analyze a regularity, which depends on the inequality of the earthquake energy releases. Particularly, we note that prior to a large earthquake, the energy released are more unequal than when such large events are not happening. Inequality in responses of a driven disordered SOC-like system is known to be useful in terms of its universal features [13, 14]. It has also shown promises, both in models [15] and (compression) fracture experiments [16], to have forecasting capabilities of imminent large events. Here, we have measured inequality of energy released within a time-window for earthquake time series in various models and also on the data from several earthquake prone regions. It is seen that in most cases, large events follow a sequence of highly unequal events quantified through elevated values of the Gini and Kolkata indices measured on such sequences.

---

\* sudip\_sarkar@srmap.edu.in

† soumyajyoti.b@srmap.edu.in

For the remaining part of the paper, we first describe the models used and the method of measuring the inequalities in their responses. We then correlate the inequalities of the responses of those models with subsequent event sizes. Finally, we analyze data from different earthquake prone regions and show that qualitatively such correlations hold there as well, indicating an underlying principle of relating response inequalities with proximity to critical point and/or lowered  $b$ -value.

## II. MODELS AND METHODS

Here, we first describe the models used for this study and then move on to define the inequality indices that are used.

### A. Sandpile-like model of earthquake

There have been many attempts to model earthquake phenomena through cellular automata type models, for example the Olami-Feder-Christensen model [17] etc. In this work, we adopt the model introduced in ref. [18]. Sandpile models typically measure event size by the number of topplings during an avalanche. The present model defines physically meaningful earthquake observables. As a result, a Gutenberg–Richter (Power) law emerges only in a specific parameter regime. We consider a two-dimensional square lattice consisting of  $N$  sites. The stress at each site increases uniformly and linearly in time at a constant rate ( $v_0$ ). When the stress at a particular site reaches a given threshold value ( $S_c$ ), an earthquake event is triggered. We choose  $D_1$  as a constant stress threshold. Sites with stress greater than  $S_c - D_1$  are identified and grouped into clusters of nearest neighbors. Only the cluster containing the triggering site participates in the earthquake. For every site in this cluster, the stress is reduced to  $S_c - D_s$ , where  $D_s = D_2 + D_3$ . Here,  $D_2$  is a fixed parameter and  $D_3$  is a random parameter. In this model "Cluster" defines a set of connected sites (grids) where stress level exceed the chosen threshold and "Avalanche" defines as a specific cluster which contains the site with maximum stress (epicenter) at that time. If  $n$  is the number of sites in this cluster then, it is related to the resulting earthquake magnitude ( $M$ ) as,

$$M = \frac{3}{2} \log n. \quad (1)$$

In our simulation, we take the internal parameter values as,  $v_0 = 1$ ,  $S_c = 10$ ,  $D_1 = 5.0$ ,  $D_2 = 10.0$ ,  $D_3 = 0.1$ , and  $N = 400$ . When the system size is large, a Gutenberg–Richter law emerges provided that

$$D_3 \ll D_1 \ll D_2$$

which means that, earthquakes involve a stress release, but the variations in stress drop are small relative to the stress level at which events are initiated. We use another spatial correlation parameter ( $D_d$ ), where the thresholds are correlated within a typical size of  $D_d^2$  (see e.g., [19]). A large value of  $D_d$  will result in a larger spatial correlation in thresholds, consequently resulting in a larger avalanche, on average. The GR and Omori-Utsu laws observed in this model were reported in ref.[18]. Here we look at the inequalities of the avalanche sizes and attempt to extract signals of imminent large events from the behavior of the inequality indices.

### B. Train model of earthquake

The train model of earthquake is a simplification of the Burridge-Knopoff model [20], where the stick-slip motion of the overlapping tectonic plates are modeled through massive blocks, connected through linear elastic springs, and driven over a rough surface. The frictional force creates the stick-slip motion and the (elastic) energy released can be measured through the motion of the blocks.

We consider a further simplification on the model [21, 22], where we take the frictional surface to be discrete set of blocks, but fixed in space. When the "train" moves over it, slowly pulled by the rightmost block ("engine"), say, some blocks of the train overlap with the fixed blocks below. At that point, they have a random pinning force that oppose the motion, and is drawn from a uniform distribution in  $(0,1)$ . The forces on a block in the train at any given instance are, therefore, the elastic forces from its nearest neighbors due to stretching of the elastic springs, and the random pinning force. If the pull due to the elastic force exceeds the random pinning, then the block is moved towards the direction of the pulling, hopping over to the next block below, only if that space is not occupied already. The train is restricted to move along the direction of pulling and never opposite.

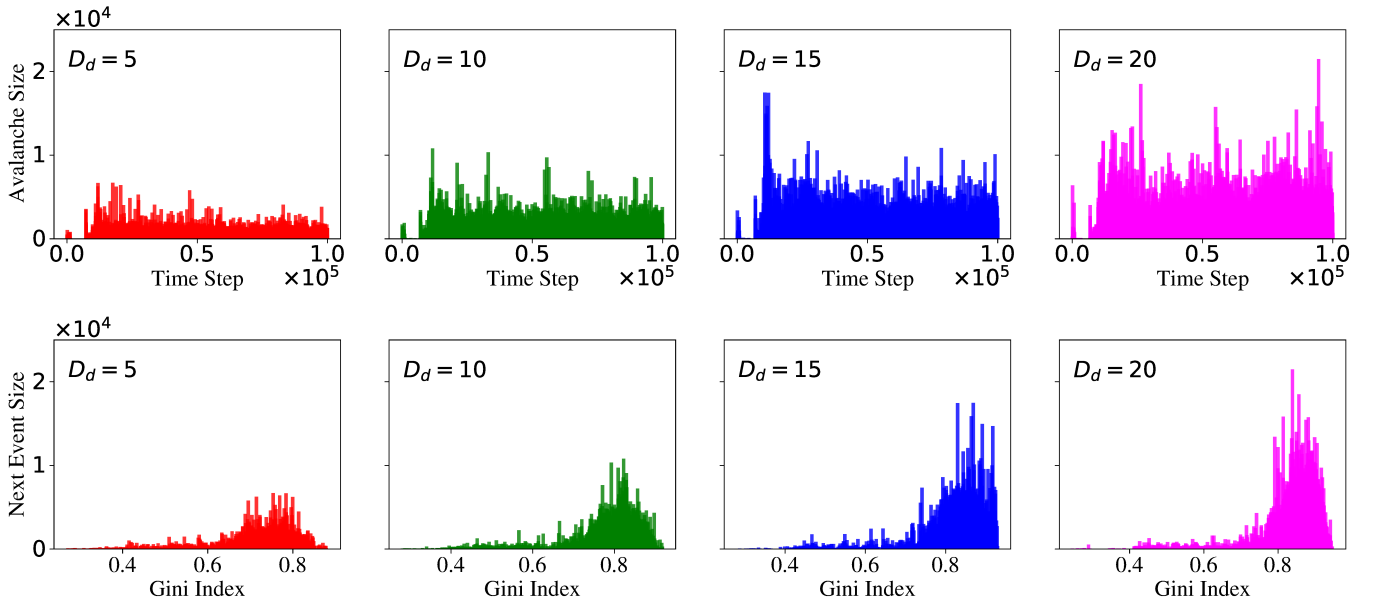


FIG. 1. The top row figures show the time series of the avalanches seen in the 2d SOC model. The bottom row figures are the same time series, but now sorted according to the  $g$  value associated with each event that are calculated from the immediately preceding 100 events. A clear correspondence is noted with high  $g$  values and large avalanches, except for the vary high  $g$  values, where event numbers are less.

The dynamics then proceeds as follows, the right most block is moved further to the right by one step and the forces are checked on all the other blocks. Some blocks might move and that can in-turn result in movements of some other blocks and so on. The rightmost block is held fixed during this re-adjustments. When all blocks stop moving, the rightmost block is moved again one step and so on. The number of blocks moving between two successive movements of the “engine” is called an avalanche. The self-organized critical dynamics of this model is well studied and can be shown to be equivalent to the quenched Edwards-Wilkinson model [23]. The avalanche size distribution follow a power-law in one and two dimensions. Here we only study the one dimensional version of the model.

### C. Inequality indices used

In quantifying the inequality of the earthquake events, in simulations and in the data, we use inequality indices that are traditionally used to quantify inequality of wealth distribution in a population, viz. the Gini [24] and Kolkata [25] indices. In measuring such indices, we need to first construct the Lorenz curve. It is done as follows: A set of numbers, here representing earthquake energy released, are first sorted in the ascending order. Then the Lorenz curve,  $L(p)$  is defined as the cumulative fraction of energy released by the smallest  $p$  fraction of the events in that sequence. Clearly,  $L(0) = 0$  and  $L(1) = 1$ . If all events were of exactly equal size, then the Lorenz curve would be a diagonal line from (0,0) to (1,1). Any departure from the diagonal line is, therefore, a measure of inequality of the events. The Gini index is defined as the area between the diagonal line and the Lorenz curve, normalized by the area under the diagonal line (1/2). Formally,  $g = 1 - 2 \int_0^1 L(p) dp$ . The value of  $g$  is always between 0 and 1, representing complete equality and complete inequality, respectively.

The Kolkata index is defined as the largest  $1 - k$  fraction of the events that accounts for the  $k$  fraction of the total energy released in the sequence. Formally, it can be obtained by solving  $1 - k = L(k)$ . It is a generalization of the Pareto’s 80-20 law in wealth (and many other) distributions, that states that 80% of wealth is typically possessed by the 20% of the richest individuals. Here it gets modified as  $1 - k$  fraction of the largest events accounts for the  $k$  fraction of the total energy released.

These measured have been used recently for systems approaching criticality and have been found to have universal features (see e.g., [26]), particularly near a critical point. Here we use these for earthquake statistics (see also [27]). The codes used for calculating the inequality indices using the different approaches are publicly available in ref. [28].

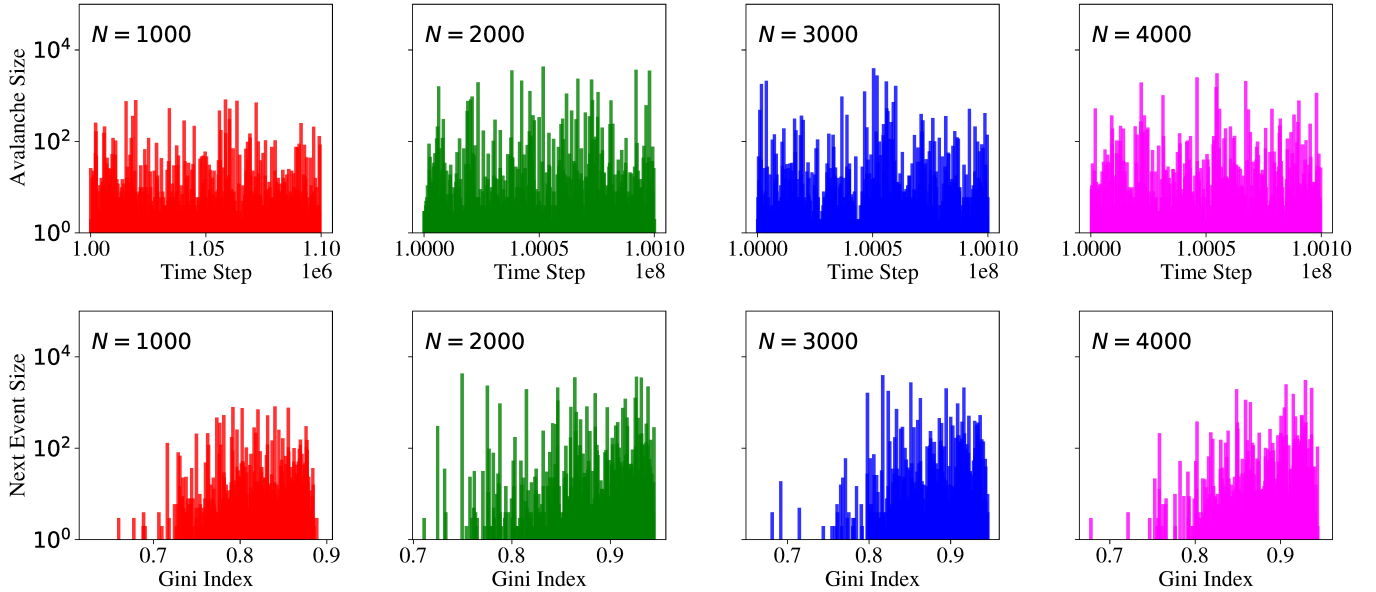


FIG. 2. The top row figures show the time series plot of the avalanches for the train model. The bottom row figures are the same series, but now sorted according to the corresponding Gini index associated with each event (calculated from the immediately preceding 100 events). The larger avalanches tend to accumulate near larger  $g$  values.

### III. RESULTS

It is known that in systems approaching a critical point, the responses tend to diverge (as does the correlation length) and the corresponding inequality measures of those responses, e.g.,  $g$  and  $k$ , become nearly equal ( $\sim 0.87$ ) shortly before the systems reach the critical points [14, 26]. For Self Organized Critical (SOC) systems as well, this behavior is seen [13], which is almost independent of the universality class of the model. Recalling that the minimum values for  $g$  and  $k$  are 0 and 0.5 respectively, the elevated inequality level of the responses from a system would indicate the proximity of a critical point and hence an imminent large response/event (see e.g., [16] for application to fracture experiments).

Here we first apply this to the 2d sandpile like model. We choose a temporal window size of  $W = 100$  consecutive events and calculate  $g$  and  $k$ . Then we assign these  $g, k$  values to the next event that immediately followed (not included) the events in the window. We then slide the window by one event and repeat the same. In this way, all events in the time series of avalanches of the model (except the first  $W$  events) will have a  $g, k$  values assigned to it that was calculated from the preceding  $W$  events. If an elevated inequality is observed prior to a large event, the  $g, k$  values attached to the larger events should be higher. In Fig. 1, the original time ordered avalanche series of the model and the same series sorted according to  $g$  values associated with the events are shown. A clear trend of accumulation of larger events towards higher  $g$  value ( $\sim 0.87$ ) is observed. A similar behavior is seen for the sorting according to the  $k$  values (see Fig.7). There are other ways to visualize this trend of unequal events preceding a large one, for example through the time series of the events superposed with the sliding window calculations of  $g, k$  (see Fig.8) and some similar other ways (see Figs.9 and 10 and the related discussions there).

Then we apply the same method to the response statistics of the train model. We choose a window of  $W = 100$  consecutive events from the time series of the avalanche sizes (mimicking energy release here) and calculate  $g$  and  $k$ . We then assign that  $g$  and  $k$  values to the event immediately following the 100 event window. We go on to do this assignments as we slide the window in time by one event each time. This means that all events, except the first 100, have inequality indices values assigned to it. Then we take all those labeled events and sort them in ascending order of the  $g$  (and  $k$ ) values. Fig. 2 shows the unsorted and the sorted time series. There is a tendency of accumulation of the larger events towards larger  $g$  value. A similar trend (see Fig.11) is observed when the sorting is done with respect to the  $k$  values. As before, the time series of  $g, k$  can also be a way to visualize this trend (see Fig.12). The cumulative energy released (see Fig.13) shows the similar trend as in the case of 2d SOC model.

Finally, we do the same exercise for the real data of earthquake catalogs in different parts of the world (Southern Japan, South-East Asia, North America and Indonesia). The coordinates used are as follows: Southern part of Japan: Minimum latitude 30.145, Maximum latitude 41.278 Min longitude 129.792, Max longitude 142.119. South East Asia: Min latitude 20.633, Max latitude 35.747 Min longitude 67.588, Max longitude 99 Western part of North America:

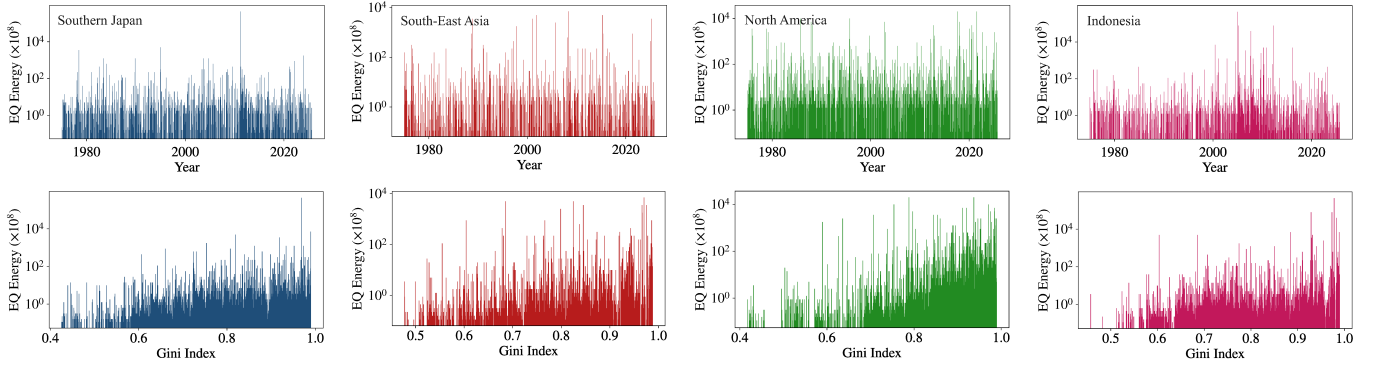


FIG. 3. Top row figures represent earthquake energy in Joule vs time for different regions. Bottom row figures represent the same events but now sorted according to their  $g$  values. The earthquake data are taken from the USGS earthquake catalog from January 1975 to October 2025. We calculate  $g, k$  indices by using a sliding window approach (see text). We convert the ISO time scale into UTC time scale and take  $W = 100$  immediate preceding an event to calculate the Gini and Kolkata indices for that event. These plots show a similar trend of accumulation of larger events for higher  $g$  values as seen in the models.

Min latitude 12.383, Max latitude 61.143 Min longitude (-145.547), Max longitude (-46.318) Indonesia: Min latitude (-7.537), Max latitude 5.703 Min longitude 95.142, Max longitude 107.051. The duration is from January 1975 to October 2025. The catalog used (USGS) can be found in [29].

First we check that the data set show Gutenberg-Richter scaling (see Fig.14). The lower cut-off used in magnitude is 4.5. Then the magnitudes are converted to energy [30] using

$$E = 10^{1.5M+C}, \quad (2)$$

where we have ignored the prefactor  $C$  as it does not influence the inequality measures. Note that inequalities in the magnitudes were reported very recently in [27]. In Fig. 3, the unsorted (actual order) and sorted (according to  $g$  values) series are shown for earthquake sequences in the different regions. Once again, a trend of accumulations of larger events towards higher  $g$  values are observed. A similar trend is observed (see Fig.15) when the events are sorted according to their  $k$  values, instead of  $g$ . The time series plots for  $g, k$  along with the events and the cumulative energy plots (see Figs.16 and 17) reflect the similar trends.

Other than the fixed sized sliding window approach, we also look at a dynamic reset approach as follows: In the earthquake energy data, we continue to measure  $g, k$  with a window size increasing with time (i.e., keep the left end fixed and move the right end of the window one event at a time). When a large event (magnitude  $\geq 7.5$ ) is encountered by the right end of the window, the left end is reset to that event and the right end is again moved one step at a time and so on. The method seeks to capture precursory events prior to a large one, which is not necessarily confined within the fixed window size considered before. Once again, higher  $g, k$  values are observed prior to large events. Note that the assignment of  $g, k$  values to an event is done similarly as before, i.e. it is assigned to the event just following (but outside) the window considered for calculating  $g, k$ . In Fig. 4, we show the events in their original (temporal) order and then in the increasing order of their  $g$  and  $k$  values. It shows a remarkable correlation between higher inequality and higher magnitude of earthquakes. In Fig. 5, we plot  $k$  vs  $g$  that gives a characteristic shape  $g = \frac{\ln(1-k) - \ln(k)}{\ln(1-k) + \ln(k)}$  known for a broad class of Lorenz curves  $L(p) = 1 - (1-p)^\theta$  (or  $L(p) = p^\theta$ ) drawn from any power law event size distribution (and is independent of the power law exponent; see [26]). We have also shown the  $g = k$  line to highlight that most of the large events happen around (generally above) it.

It is important to explore the relation between the elevated values of the inequality indices and a decrease in the so called  $b$ -value and the proximity to a critical point. It is known that for a power-law size distributed events, say following  $P(S) \sim S^{-\beta}$ , if the events are arranged in ascending order of their sizes (with  $r$  denoting the index of ordering), it will show a diverging function such as  $S_r \sim (r - r_0)^{-n}$ , where the diverging/system spanning event happens at  $r = r_0$ , with  $n = \frac{1}{\beta-1}$  (see e.g., [31]). For a system driven towards a failure/transition, the natural order is often close to the ascending order. For systems with near stationary sequences, precursory events show a growing rate of energy release prior to large events (see e.g., [16]). Therefore, a reasonable assumption is the (nearly) ascending order of events prior to a large event (see e.g., [32]). It is then possible to calculate the Lorenz function and consequently the Gini index in the closed form [14]:

$$g(x, n) = 1 - \frac{2}{1 - (1-x)^{1-n}} \left[ 1 + \frac{(1-x)^{2-n} - 1}{(2-n)x} \right], \quad (3)$$

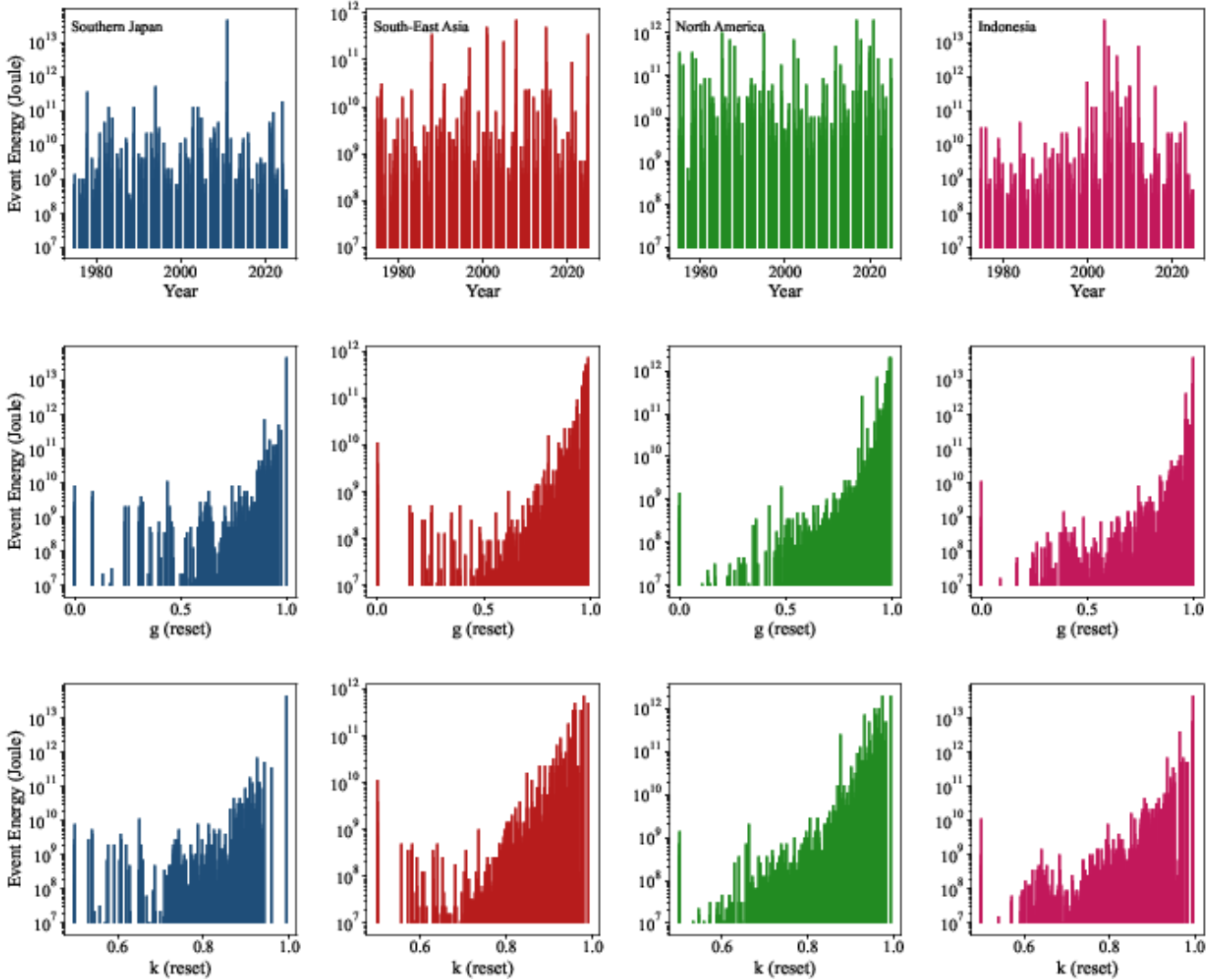


FIG. 4. The top row figures show the earthquake events in their original order of occurrence, the middle and bottom row figures show the same events when arranged in terms of their associated  $g$  and  $k$  values respectively, where the  $g$  and  $k$  values for any event is calculated from a dynamic time window defined as all events between the previous large ( $M \geq 7.5$ ) event and the current event (excluding both the ends). A clear correlation between higher inequality and larger magnitude is seen for each of the tectonically active region.

where  $x = 1$  at the critical point. It can be interpreted as a dimensionless parameter indicating proximity to critical point (for example,  $T/T_c$  in magnetic systems,  $\sigma/\sigma_c$  in fracture models and so on). A similar interpretation applied for SOC systems even though such parameters are not explicitly tuned in those systems (e.g., some form of normalized height  $h/h_c$  in sandpiles). In Fig. 6, we plot the variation of  $g$  as a function of  $n$  (hence,  $\beta$ ) for different values of  $x$ . Within the plot, we indicate the  $g$  values obtained through the reset method mentioned above. Note that an increase in the  $g$  value would correspond to either an increase in  $n$  (implying a lowering of  $\beta$  or  $b$ -value) or a closer proximity to the critical point (increase in  $x$ ), or both. Therefore, the lowering of  $b$ -value, observed for many large earthquakes [8], is consistent with increase in the inequality of event sizes prior to a large event. Even though a range in the  $n$  values is indicated from the error margin of fitting the GR law from the data, the changes in the exponent could be more than the range, but is generally difficult to estimate for few events (for example,  $W = 100$  here).

The intersection area of the two rectangular regions in Fig. 6 indicating the observed  $g$  (within one standard deviation) and  $n$  (within fitting error bars) values depict the area where the tectonic plate system is likely to reside over the course of the dynamics. The time series plots of  $g$  and  $k$  evolution and event sizes with time is included in Fig.18. As expected in the case of an attractive fixed point at criticality, a characteristic of SOC dynamics, the system is always very close to the critical point  $x = 1$ .

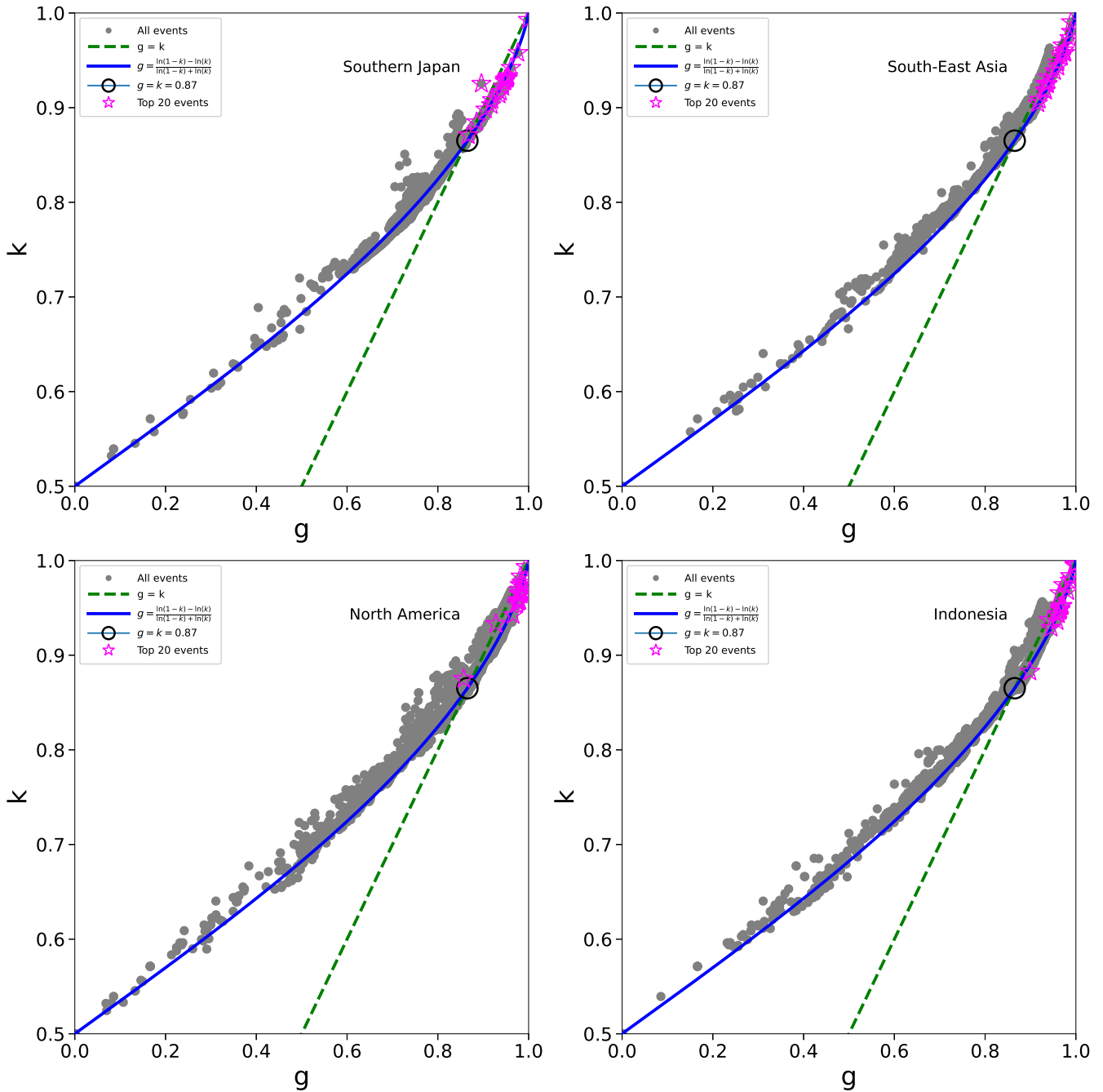


FIG. 5. The  $g$  and  $k$  values obtained from the dynamic reset method (see text) are plotted and the largest 20 events are highlighted. All of the largest 20 events happen around  $g \approx k$  and for higher values of the inequality indices. The time variations of  $g, k$  and the corresponding event series are shown in the Fig.18.

#### IV. DISCUSSIONS AND CONCLUSION

The inequalities of the earthquake energy released, in models and data, show a consistent trend of the larger events following a set of highly unequal ones. This is seen in the two models studied here: a 2d SOC like model [18] and the train model of earthquake [22], and also in data taken from various earthquake prone zones around the world. While earthquake dynamics have been cast in the form of SOC dynamics over many years, there are some persistent doubts as well. However, at least for the behavior of inequality indices such dynamics seem to follow the near universal trend observed in the SOC models [13] (see also discussions on Fig. 6 above).

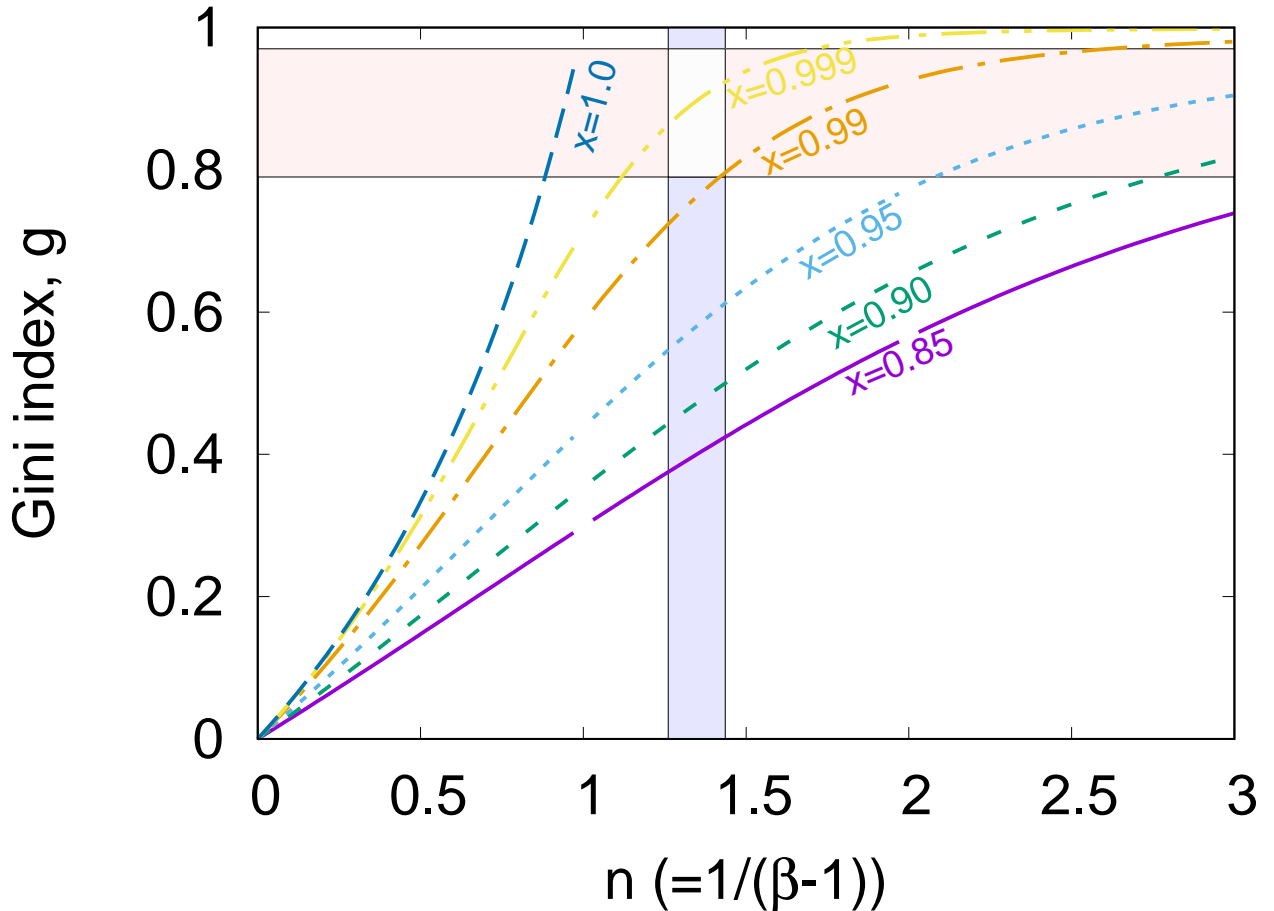


FIG. 6. The variations of the Gini index ( $g$ ) are shown with  $n$  (hence, the event size distribution exponent  $\beta$ ) for various values of the parameter  $x$  that denotes proximity to a critical point ( $x = 1$  is the critical state; see text for details). The shaded horizontal rectangle denotes the range of  $g$  values observed in the dynamic reset (see Fig. 5) method:  $\langle g \rangle \pm \sigma_g$ , where  $\langle g \rangle = 0.88$  is the average and  $\sigma_g = 0.09$  is the standard deviation. The shaded vertical rectangle denotes the range of  $n$  (calculated from the range of  $\beta$  obtained in the GR law fit; see Fig.14). The overlapping shaded area is an indicator where the system might residing be during the course of the dynamics, and it is always very close to the critical point, as is conjectured in an SOC picture of tectonic plates.

In the context of earthquakes, this also aligns with the earlier observation of lowering of the size distribution exponent prior to large events (see e.g., [7, 8]). A lowering of exponent necessarily means an increase in the inequality of the events (see Fig. 6). Therefore, in that context, this current observation can provide an alternative to fitting the exponent values from a limited data set and just calculating their inequality could work in providing a potential hazard analysis. On the same note, the estimates of the GR law exponent and the measured values of  $g$  together suggest a very close proximity of the model from a critical point (see Fig. 6). While this is not a rigorous proof, it gives an indication of SOC like dynamics in tectonic dynamics in a quantitative manner. On the other hand, a close proximity to the critical point tends to increase the inequality in response preceding events that are not necessarily always very large in comparison to other events in a different part of the tectonic plate, since that would depend on the specific areas of the plate boundaries considered. The inequality indices considered here don't depend on the absolute sizes of the events, but only depend on the functional form they follow. Therefore, we notice many small events for large  $g, k$  values that could be large compared to the other local events but not large globally. However, for the most part, large events do not occur for small  $g, k$  values. The elevated  $g, k$  values prior to a large event is also consistent with significant increase in the event and energy release rates, which were observed for earthquakes [32] and also more recently for compression failure of nano porous materials [16].

In conclusion, we have studied earthquake energy size inequalities in models and real data for some tectonically active areas around the world and found consistent evidence that the earthquake sizes, measured in terms of energy released, become highly unequal prior to a large event. This can lead to potential earthquake hazard analysis in the

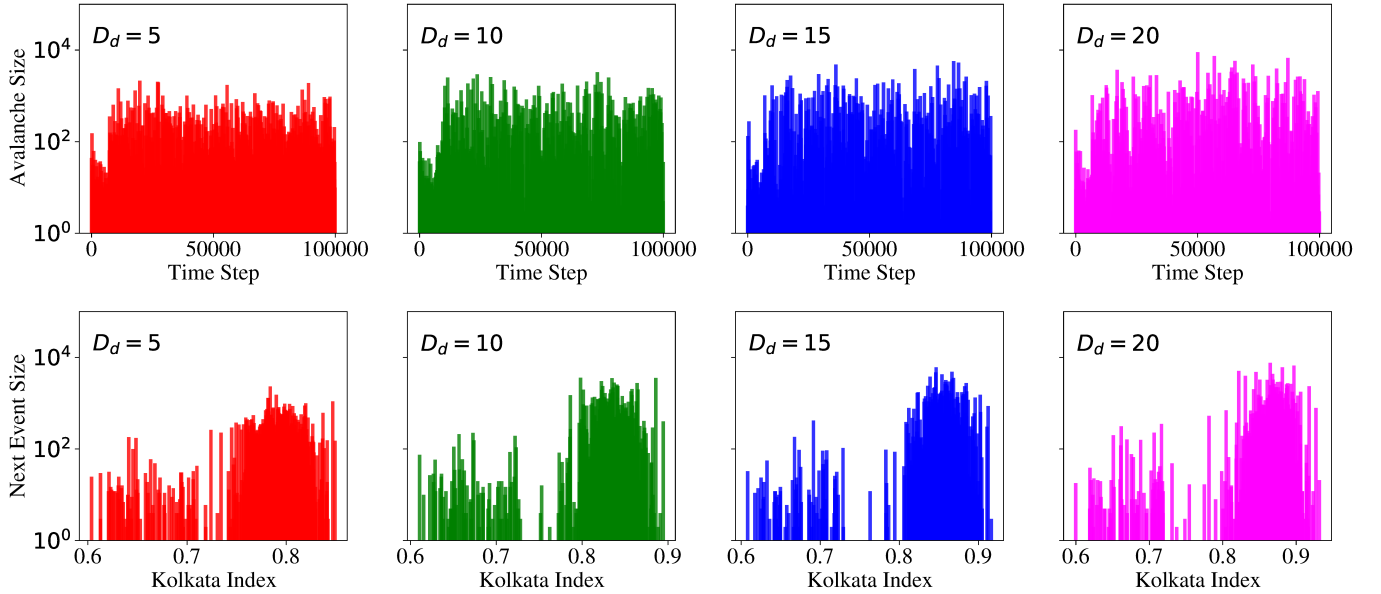


FIG. 7. The top row shows the avalanche size time series for the 2d SOC model with different values of the correlation length  $D_d$  of the disorder. The bottom row shows the exact same time series, however now they are arranged by the Kolkata index value (measured for a sliding window of size  $W = 100$  of the preceding  $W$  events). Like in the case of sorting with the Gini index value, this shows a tendency of larger events accumulating for larger  $k$  values.

future.

## V. APPENDIX A: INEQUALITY OF AVALANCHES IN THE 2D SOC MODEL

As described in the main text, we have performed numerical simulations of the 2d SOC model and studied the inequalities of the the resulting avalanches, particularly near the large avalanches. The sliding window calculations of  $g$  and  $k$ , as mentioned in the main text, assign a  $g$  and  $k$  value to each event that are calculated from the preceding  $W = 100$  events. The sorting of the events according to  $g$  values are shown in the main text, the sorting according to the  $k$  values are shown in Fig. 7, showing a similar trend of accumulation of large events near large  $k$  values, as in the case of  $g$ .

Another way to visualize the correspondence of the event sizes with the preceding inequality of the same, is to look at the time variation of the inequality indices along with the time series of the (avalanche) events. For the 2d SOC model, such a variation is shown in Fig. 8, for various values of the correlation parameter  $D_d$ .

One can also note the event sizes in the 2d SOC model through the corresponding cluster size (of sites higher than the failure threshold) corresponding to the events. These are also power law distributed and show a similar behavior in terms of the inequality indices. In Fig. 9, we plot the time variation of the cluster sizes corresponding to the events and the  $g, k$  values, again calculated using a sliding widow of size  $W = 100$ .

We have measured the total energy released (in this case the total avalanche event size) within a range of  $g$  values (with bin size 0.01), which indicates a systemic increase in the cumulative energy (avalanche) as a function of  $g$ . A sharp decrease for very high  $g$  values is seen (see Fig. 10), as there are hardly any events in that range.

## VI. APPENDIX B: INEQUALITY OF AVALANCHES IN THE TRAIN MODEL

As described in the main text, we have performed numerical simulation of the avalanches in the train model for different system sizes. The inequality of the avalanche sequence was measured using a sliding window approach of window size  $W = 100$ , and each event was assigned  $g, k$  values, calculated from the immediately preceding 100 events. The main text describes sorting of the events with  $g$  values, here we show the sorting with  $k$  values (see Fig. 11). A similar tendency of accumulation of larger events for higher  $k$ , mainly for the larger system size simulations, is observed.

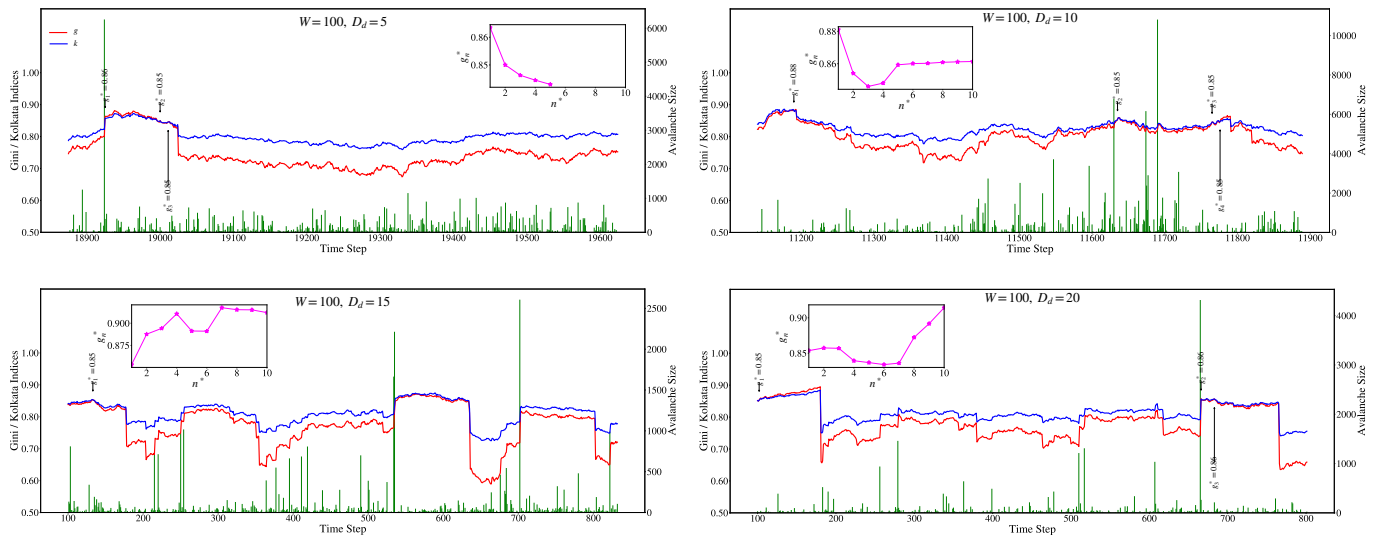


FIG. 8. The time variation of  $g$  and  $k$  are shown for the avalanche time series for different values of the correlation parameter  $D_d$  in the 2d SOC model. The two indices become nearly equal before large events (as indicated), particularly for larger values of the correlation parameter. Insets show the  $g$  values when it crossed  $k$  for the first 10 times. Only a part of the total sequence is shown for clarity, which do not include all the crossings.

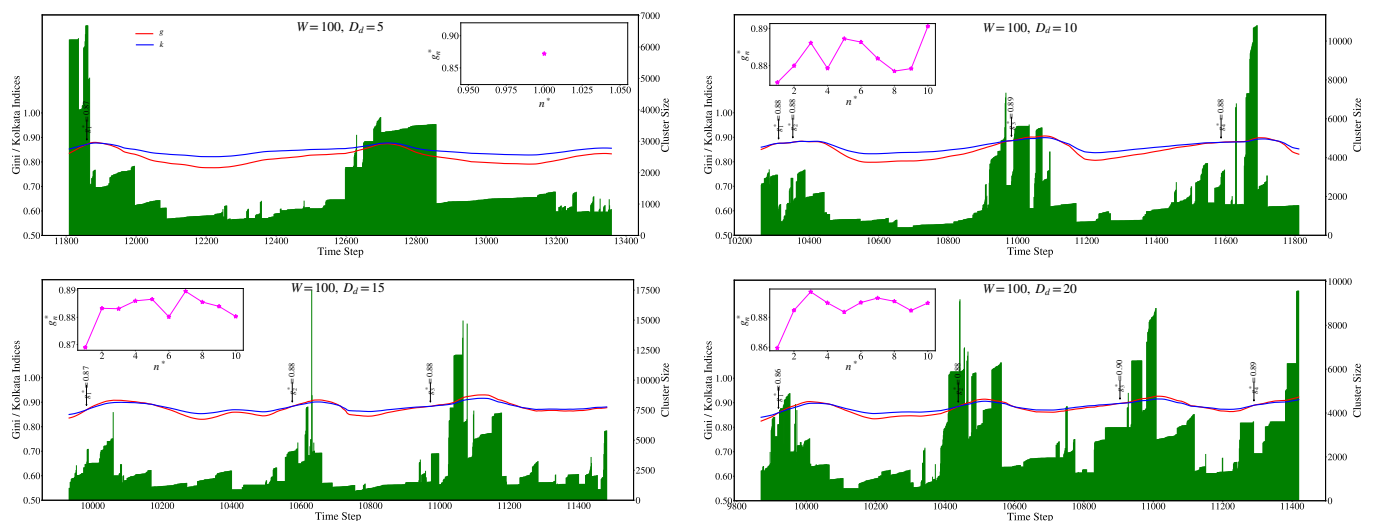


FIG. 9. The time variation of  $g$  and  $k$  are shown for the cluster series for different values of the correlation parameter  $D_d$  in the 2d SOC model. The two indices become nearly equal before large events (as indicated), particularly for larger values of the correlation parameter. Insets show the  $g$  values when it crossed  $k$  for the first 10 times. Only a part of the total sequence is shown for clarity, which do not include all the crossings.

As above, we can also see here the time variation of the inequality of the avalanches and the event sizes (see Fig. 12) in the train model. The two indices,  $g$  and  $k$  become nearly equal prior to large events, particularly for the larger system size simulations.

We also measure the cumulative avalanche sizes with  $g$  with a bin size of 0.01, in the train model (see Fig. 13). As in the earlier case, there is a systemic increase of the cumulative size (not normalized by event count) as a function of  $g$ .

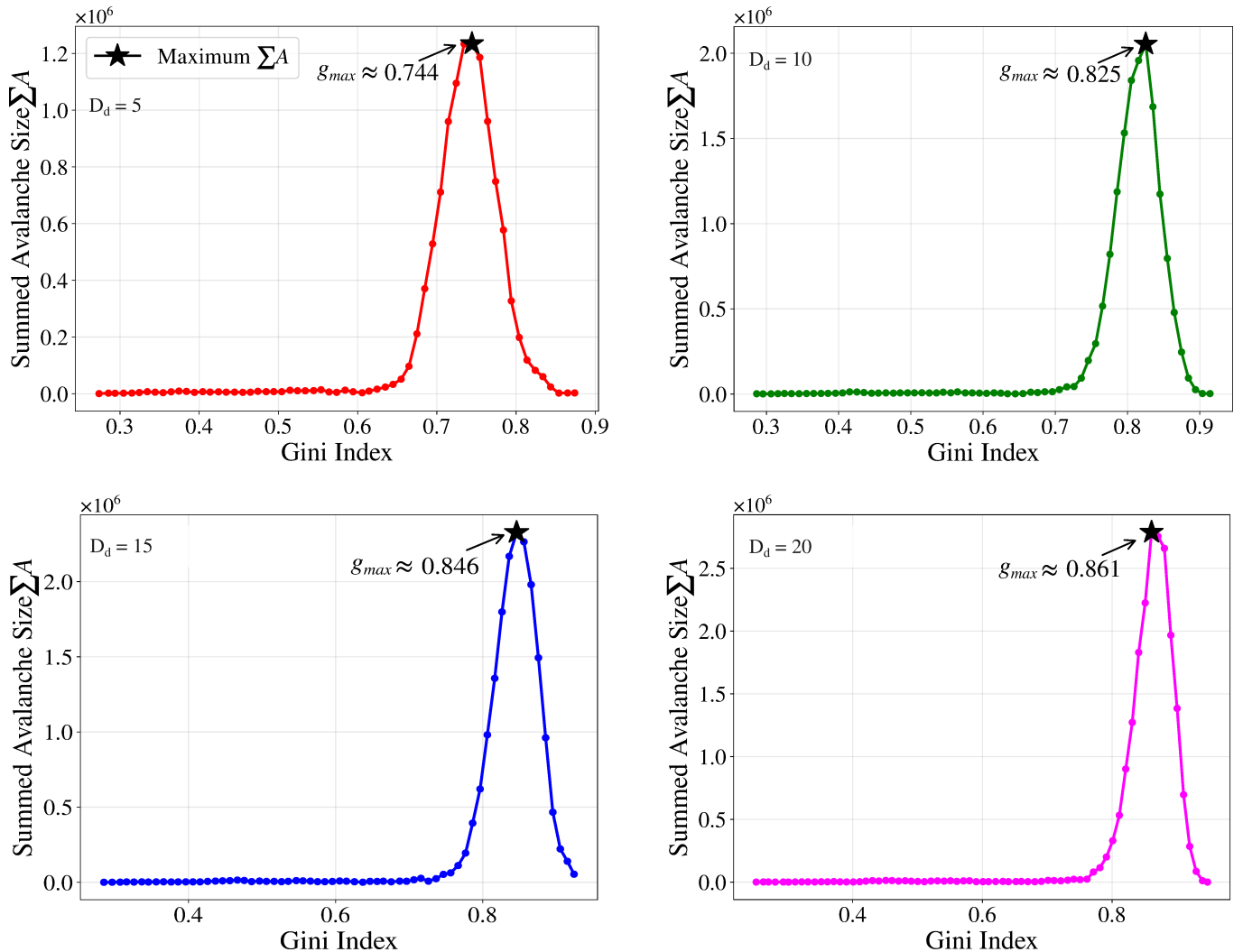


FIG. 10. The total size of avalanche (a measure for energy released) is shown as a function of  $g$  with a binning window size 0.01 for different values of the correlation parameter  $D_d$  for disorder in the 2d SOC model. A systemic increase with  $g$  is noticed, except for very high values of  $g$ , where there is hardly any event. The cumulative avalanche size is not normalized by event number, which is another reason for a very sharp rise.

## VII. APPENDIX C: INEQUALITY OF ENERGY RELEASED IN EARTHQUAKES

As mentioned in the main text, we analyze earthquake data, obtained from the USGS catalog, for different earthquake prone regions. We note the magnitudes of the events and first convert it to energy. Then we analyze the inequality in terms of the energy released, since it is the energy that are distributed in a power law.

Before such analysis, it is important, however, to check the Gutenberg-Richter law, to check the completeness of the data set. We have set a lower threshold of magnitude 4.5 for considering the events. Then the size distribution of the corresponding energies follow the Gutenberg-Richter power law (see Fig. 14). The fitting exponent for the individual regions and total data of all the regions together are shown. It is from this range of the exponent values obtained for the individual regions that constitute the range in  $n$  in Fig. 5 in the main text.

As mentioned in the main text, we calculated the inequality of the energy released using a sliding window approach of window size  $W = 100$ . In Fig. 15, we show the sorting of the events according to the  $k$  values (calculated from the immediately preceding 100 events) associated with each event. A tendency of accumulation of larger events to higher  $k$  values is observed, as in the case of sorting with  $g$  (see main text).

We can also visualize the time variation of the inequality indices, calculated through a sliding window approach of size  $W = 100$ , and the corresponding energy released. In Fig. 16, such variations are plotted for the earthquakes of different regions.

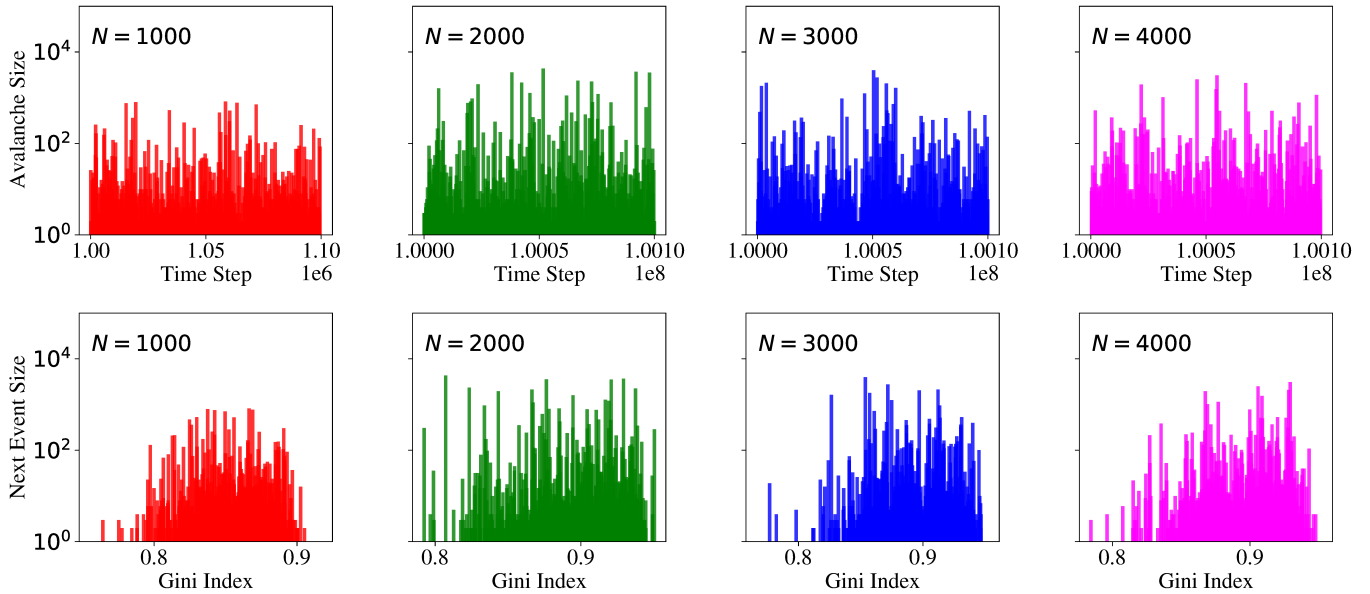


FIG. 11. Top row shows the avalanche size time series for the train model with different system sizes ( $N$ ). The bottom row shows the same exact time series when the events are sorted according to the associated Kolkata index ( $k$ ) value (calculated from the immediately preceding  $W = 100$  events). A tendency of accumulation of larger events for larger  $k$  values is seen, especially for the  $N = 4000$  system size, similar to what was seen with the same exercise with the Gini index, as mentioned in the main text.

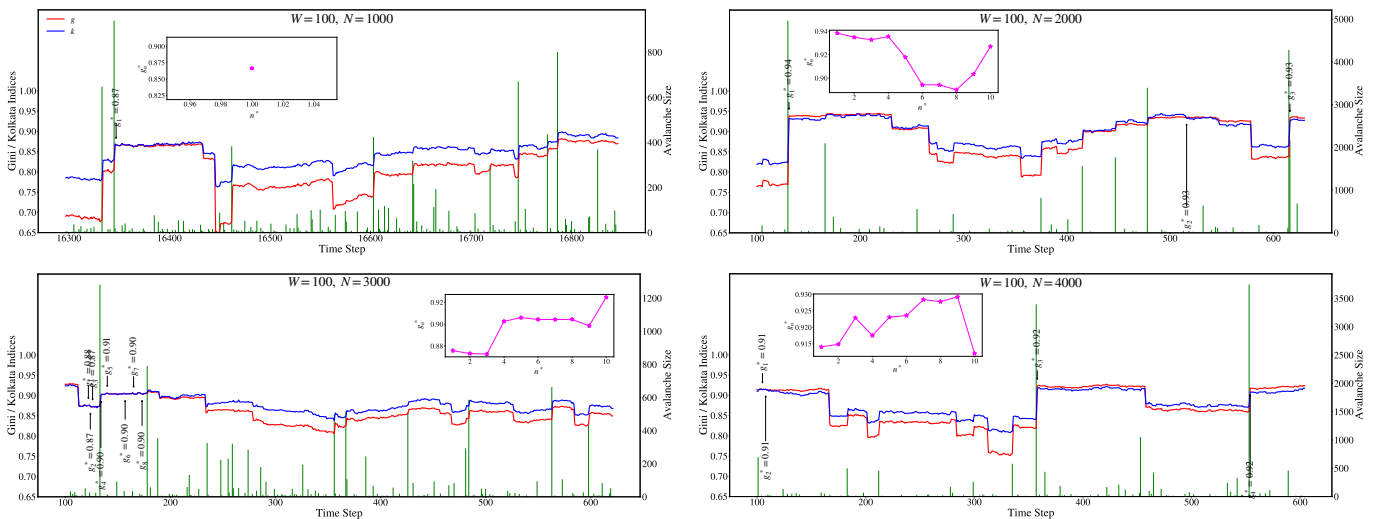


FIG. 12. The time variation of  $g$  and  $k$  are plotted along with the corresponding avalanches for the train model with different system sizes. The crossing of  $g$  and  $k$  are indicated. The two indices,  $g$  and  $k$  become nearly equal prior to large events. Insets show the values of  $g$  for the first 10 times it crossed  $k$ . Only a part of the total sequence is shown for clarity, which does not include all the crossings.

As in the case of the models, we have measured the cumulative energy released as a function of  $g$ , with a bin size of 0.01. The resulting plots (see Fig. 17) show sharp increase for higher  $g$  values.

In Fig. 18 we show the variation of the  $g, k$  values with time, when the calculations are done through a dynamical reset rule (see text) of resetting the window every time a large (greater than or equal to magnitude 7.5) event occurs.

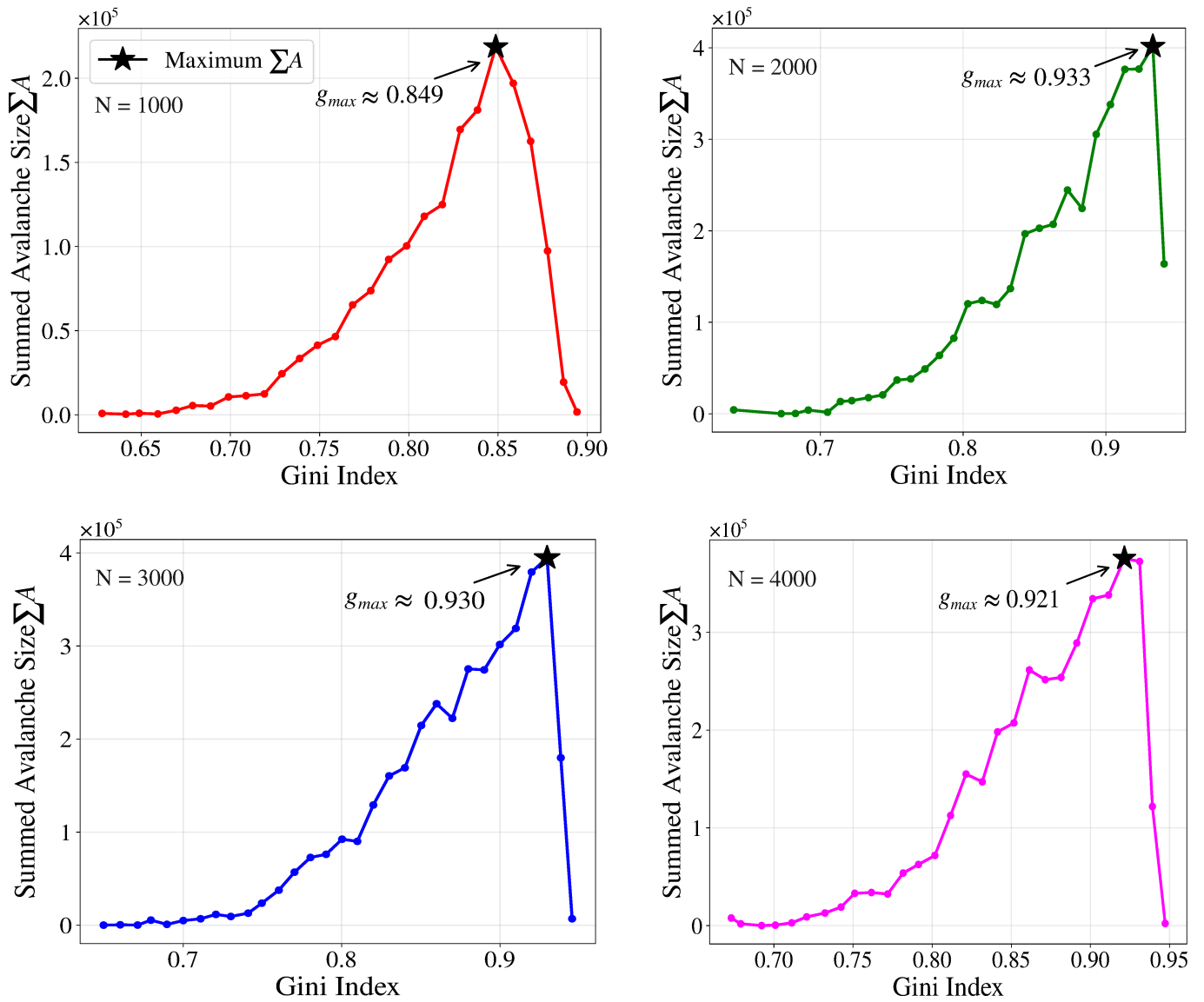


FIG. 13. The variations of the cumulative avalanche with  $g$ , measured for a bin size of 0.01, are shown for the different system sizes of the train model. A systemic increase for larger  $g$  values are seen, as before.

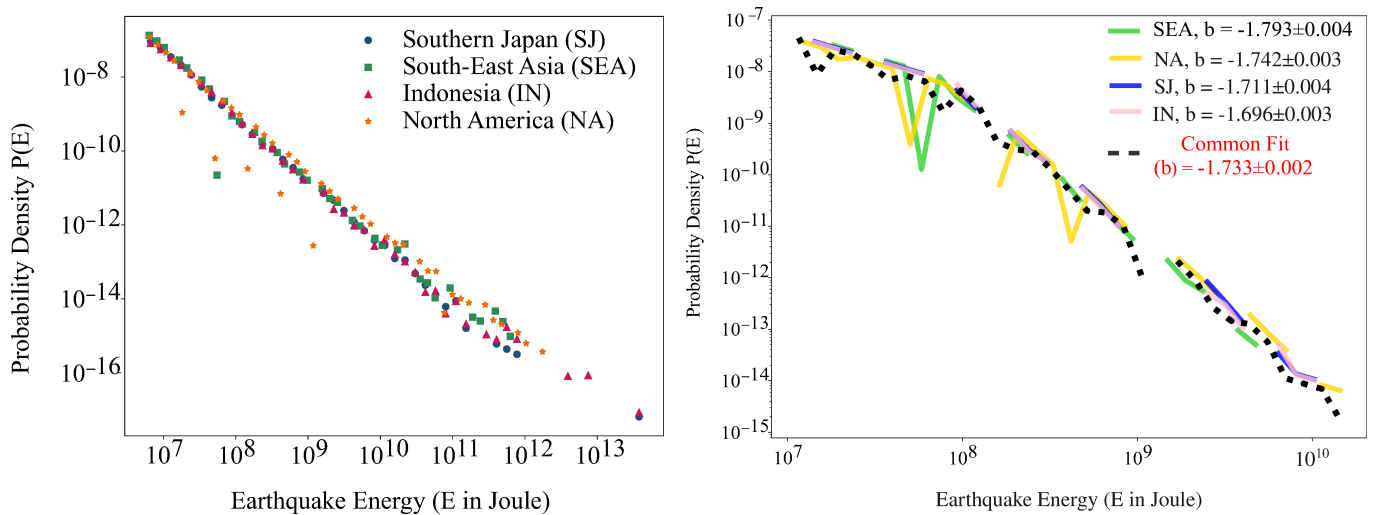


FIG. 14. The probability distributions of the energy released in the earthquakes for the various regions are shown to fit the Gutenberg-Richter power law.

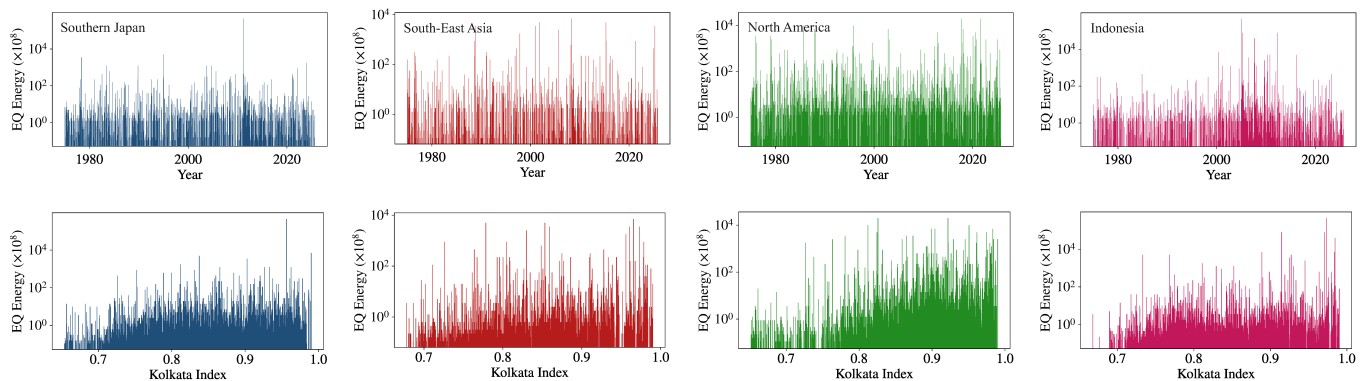


FIG. 15. The top row figures show the time series of energy released in earthquakes in different regions and the bottom row figures show the same series when sorted according to the associated  $k$  value for each event, calculated from the preceding 100 events in time. As in the case of  $g$  (see main text), a tendency of accumulation of the larger events to higher  $k$  values is observed.

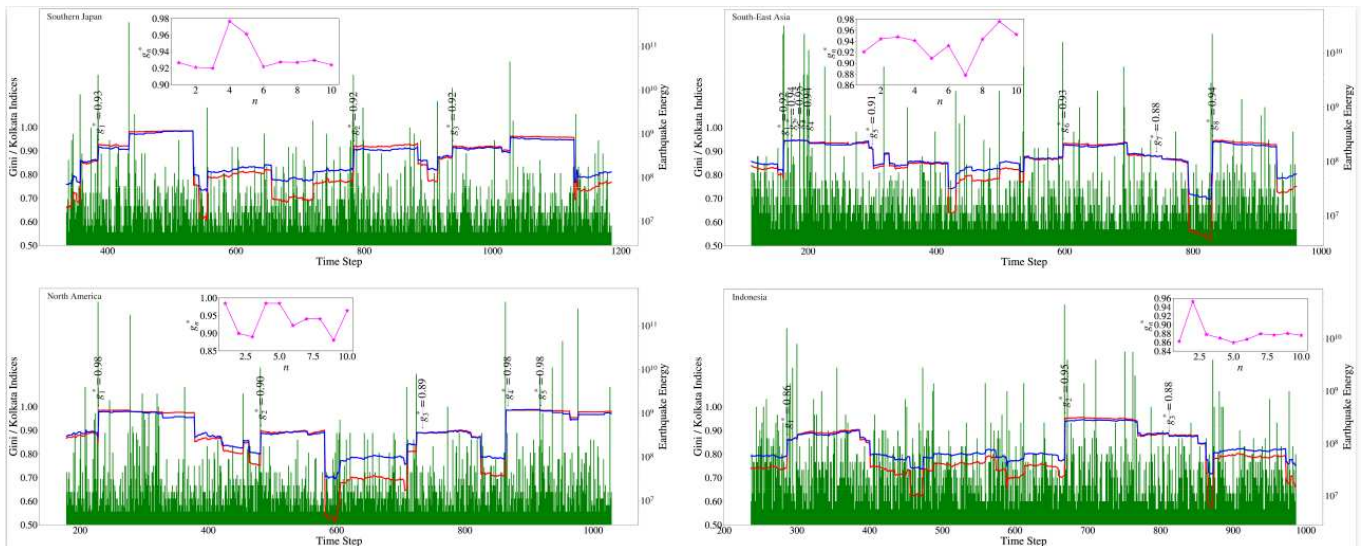


FIG. 16. The time series plots of  $g, k$  are shown for the different earthquake prone regions with a sliding window of size  $W = 100$ . Insets show the  $g$  values when it crossed  $k$  for the first 10 times. Only a part of the total sequence is shown for clarity, which do not include all the crossings.

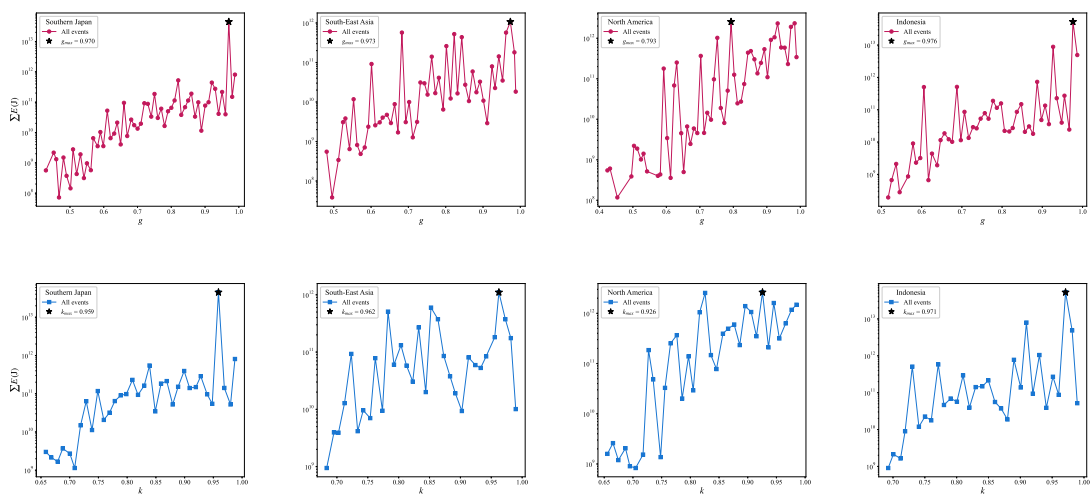


FIG. 17. The cumulative energy released in the earthquakes of the different regions studied are shown for a bin size 0.01. The total energy is not normalized by the event count.

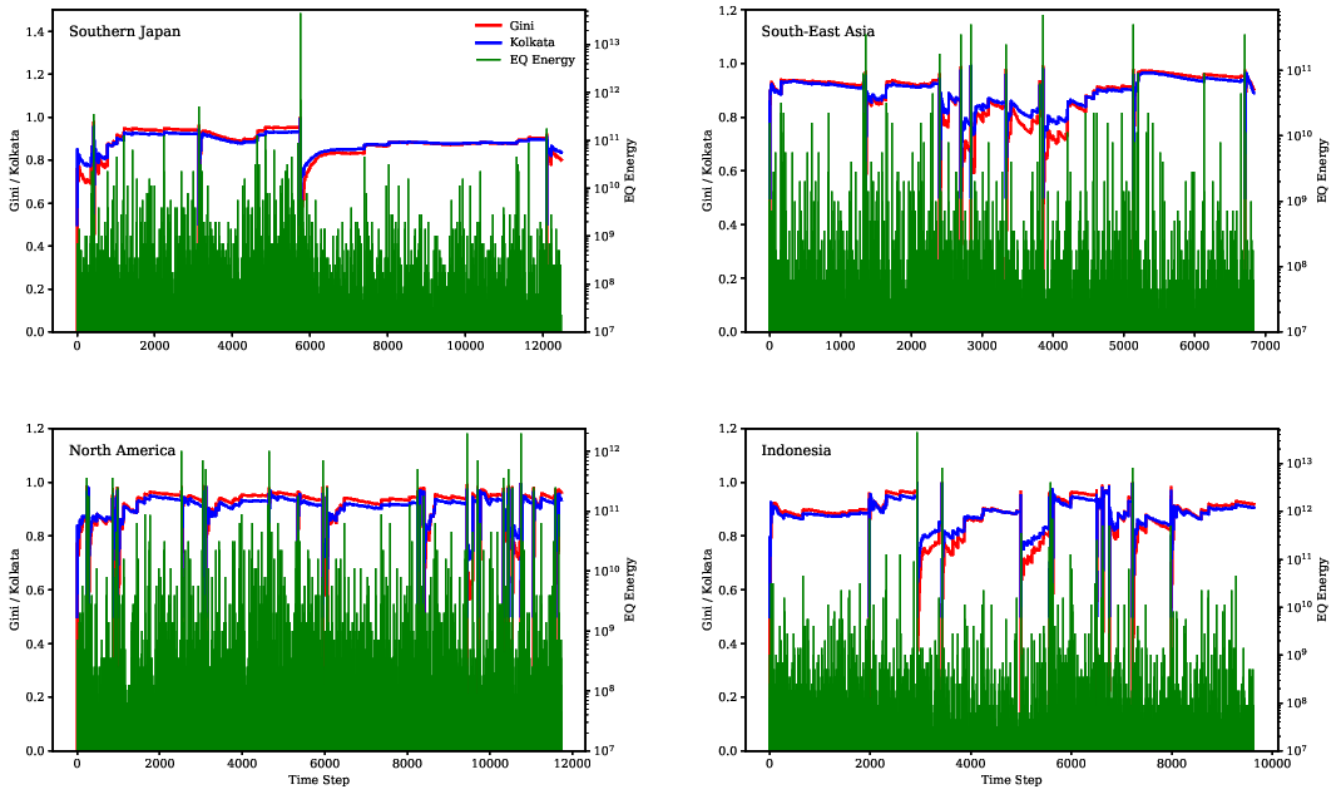


FIG. 18. The time evolution of the  $g, k$  indices are shown with dynamic reset (following an event of magnitude 7.5 or higher) with the corresponding event sizes. This shows the inequality indices increasing significantly prior to the large events. Only a part of the time series are shown in each region.

## VIII. ACKNOWLEDGEMENTS

We thank Bikas K. Chakrabarti and Takahiro Hatano for fruitful discussions. The simulations were performed in HPCC Chandrama at SRM University - AP.

- 
- [1] J. M. Carlson, J. S. Langer, and B. E. Shaw, *Dynamics of earthquake faults*, Rev. Mod. Phys. **66**, 657–670 (1994).
- [2] H. Kawamura, T. Hatano, N. Kato, S. Biswas, and B. K. Chakrabarti, *Statistical physics of fracture, friction, and earthquakes*, Rev. Mod. Phys. **84**, 839–884 (2012).
- [3] B. Gutenberg and C. F. Richter, *Frequency of earthquakes in California*, Bull. Seismol. Soc. Am. **34**, 185–188 (1944).
- [4] F. Omori, *On the aftershocks of earthquake*, J. Coll. Sci. Imp. Univ. Tokyo. 1894. P. 111–200.
- [5] T. Utsu, Y. Ogata, R. S. Matsu'ura, *The centenary of the Omori formula for a decay law of aftershock activity*, J. Phys. Earth **43**, 1–33 (1995).
- [6] C. H. Scholz, *The frequency-magnitude relation of microfracturing in rock and its relation to earthquakes*, Bull. Seismol. Soc. Am. **58**, 399–415 (1968).
- [7] H. Kawamura, H., 2006, in Modelling Critical and Catastrophic Phenomena in Geoscience, edited by P. Bhattacharyya, and B. K. Chakrabarti (Springer-Verlag, Heidelberg), pp. 223–257.
- [8] K. Z. Nanjo, N. Hirata, K. Obara, K. Kasahara, *Decade-scale decrease in  $b$  value prior to the M9-class 2011 Tohoku and 2004 Sumatra quakes*, Geophys. Res. Lett. **39**, L20304 (2012).
- [9] T. Hatano, C. Narteau, P. Shebalin, *Common dependence on stress for the statistics of granular avalanches and earthquakes*, Sci. Rep. **5**, 12280 (2015).
- [10] J. B. Rundle, S. Stein, A. Donnellan, D. L. Turcotte, W. Klein, C. Saylor, *The complex dynamics of earthquake fault systems: new approaches to forecasting and nowcasting of earthquakes*, Rep. Prog. Phys. **84**, 076801 (2021).
- [11] P. A. Varotsos, N. V. Sarlis, T. Nagao, *Complexity measure in natural time analysis identifying the accumulation of stresses before major earthquakes*, Sci. Rep. **14**, 30828 (2024).
- [12] M. Luginbuhl, J. B. Rundle, D. L. Turcotte, *Statistical physics models for aftershocks and induced seismicity*, Phil. Trans. R. Soc. A **377**, 2136 (2019).
- [13] S. S. Manna, S. Biswas, B. K. Chakrabarti, *Near universal values of social inequality indices in self-organized critical models*, Physica A **596** 127121 (2022).
- [14] S. Das and S. Biswas, *Critical scaling through Gini index*, Phys. Rev. Lett. **131**, 157101 (2023).
- [15] S. Biswas and B. K. Chakrabarti, *Social inequality analysis of fiber bundle model statistics and prediction of materials failure*, Phys. Rev. E **104**, 044308 (2021).
- [16] Diksha, J Baró, S Biswas, *Inequalities of energy release rates in compression of nano-porous materials predict its imminent breakdown*, Phys. Rev. E **111**, L053502 (2024).
- [17] Z. Olami, H. J. S. Feder, K. Christensen, *Self-organized criticality in a continuous, nonconservative cellular automaton modeling earthquakes*, Phys. Rev. Lett. **68**, 1244 (1992).
- [18] F. Pétrélis, K. Chanard, A. Schubnel, and T. Hatano, *Stress spatial distributions, the Gutenberg–Richter and Omori–Utsu laws*, J. Stat. Mech. **2024**, 043404 (2024).
- [19] O. Borgman, P. Fantinel, W. Lühder, L. Goehring, R. Holtzman, *Pore scale study of drying in spatially correlated porous media*, Water Resour. Res. **53**, 5645–5658 (2017).
- [20] R. Burridge and L. Knopoff, *Model and theoretical seismicity*, Bull. Seismol. Soc. Am. **57**, 341 (1967).
- [21] M. Vieira, *Self-organized criticality in a deterministic mechanical model*, Phys. Rev. A **46**, 6288 (1992).
- [22] S. Biswas, P. Ray, and B. K. Chakrabarti, *Equivalence of the train model of earthquake and boundary driven Edwards–Wilkinson interface*, Eur. Phys. J. B **86**, 388 (2013).
- [23] S. F. Edwards and D. R. Wilkinson, *The surface statistics of a granular aggregate*, Proc. R. Soc. Lond. A **381**, 17–31 (1982).
- [24] C. Gini, *Measurement of inequality of incomes*, Econ. J. **31**, 124–126 (1921).
- [25] A. Ghosh, N. Chattopadhyay, and B. K. Chakrabarti, *Inequality in societies, academic institutions and science journals: Gini and  $k$ -indices*, Physica A **410**, 30–34 (2014).
- [26] A. Ghosh, S. Biswas, and B. K. Chakrabarti, *Success of social inequality measures in predicting critical or failure points in some models of physical systems*, Front. Phys. **10**, 990278 (2022).
- [27] S. Sen, S. Banerjee, and B. K. Chakrabarti, *Relations among different inequality measures in complex systems: From kinetic exchange to earthquake models*, arXiv:2512.18408 [physics.soc-ph] (2025).
- [28] The codes used for calculating  $g$  and  $k$  using the different approaches are publicly available in: [https://github.com/soumya-84/gk\\_earthquake](https://github.com/soumya-84/gk_earthquake)
- [29] The data for the indicated regions were obtained for the duration between January 1975 to October 2025 and is downloaded from: <https://earthquake.usgs.gov>
- [30] P. Bormann and D. Di Giacomo, *The moment magnitude  $M_w$  and the energy magnitude  $M_e$ : Common roots and differences*, J. Seismol. **15**, 411–427 (2011).
- [31] Diksha, G. Eswar, S. Biswas, *Prediction of depinning transitions in interface models using Gini and Kolkata indices*, Phys. Rev. E **109**, 044113 (2024).
- [32] M. Bouchon, V. Durand, D. Marsan, H. Karabulut, J. Schmittbuhl, *The long precursory phase of most large interplate earthquakes*, Nat. Geosci. **6**, 299 (2013).